



Local microarchitecture affects mechanical properties of deposited extracellular matrix for osteonal regeneration

M. Pilia*, T. Guda, B.E. Pollot, V. Agüero, M.R. Appleford

Department of Biomedical Engineering, University of Texas at San Antonio, San Antonio, TX, USA



ARTICLE INFO

Article history:

Received 13 July 2013

Received in revised form 23 September 2013

Accepted 19 October 2013

Available online 31 October 2013

Keywords:

Cortical bone

Microchannels

Extracellular matrix

Hydroxyapatite

Nanoindentation

ABSTRACT

Multiple biomimetic approaches have been attempted to accelerate the regeneration of functional bone tissue. While most synthetic scaffolds are designed to mimic the architecture of trabecular bone, in the current study, cortical bone like extracellular matrix was regenerated *in vitro* within organized structures. Biphasic calcium phosphate (BCaP) and hydroxyapatite (HAp) scaffolds were developed with longitudinal microchannels (250 μm diameter) that resembled native osteons in cortical bone. BCaP and HAp scaffolds had a compressive strength of 7.61 ± 1.42 and 9.98 ± 0.61 MPa respectively. The constructs were investigated *in vitro* to evaluate the organization and stiffness of the extracellular matrix (ECM) formed by human fetal osteoblasts (HFOBs) cultured inside the microchannels. The ECM deposited on the BCaP scaffolds was found to have a higher micro hardness (h) (1.93 ± 0.40 GPa) than the ECM formed within the HAp microchannels ($h = 0.80 \pm 0.20$ GPa) ($p < 0.05$) or native bone ($h = 0.47 - 0.74$ GPa). ECM deposition within the microchannels resembled osteoid organization and showed a significant increase in both osteoid area and thickness after 24 days ($p < 0.001$). These observations indicate that controlled microarchitecture, specifically cylindrical microchannels, plays a fundamental role in stimulating the appropriate cellular response aimed at recreating organized, cortical bone like matrix. These findings open the door for researchers to develop a new generation of cortical bone scaffolds that can restore strong, organized bone.

© 2013 Elsevier B.V. All rights reserved.

1. Introduction

Natural bone derives much of its mechanical strength from cortical bone, specifically through the organization of its osteons. These microchannel like structures are found throughout cortical bone and are organized in concentric layers (lamellae). Type I collagen (Col I), the major organic component of bone, is secreted by osteoblasts during osteonal development, forming the underlying lamellar structure. Secretion of collagen at alternating orientations, followed by mineralization, gives bone its high compressive strength and toughness [1]. This process is characterized by the secretion of calcium phosphates (CaP) crystals by osteoblasts that are then deposited within the extracellular matrix (ECM) [2]. Bone minerals and other inorganic components give bone its hardness, whereas the organic component gives it elasticity [3]. As a result of this organization, bone is a very tough structure, with cortical bone capable of reaching a compressive strength ranging between 100–230 MPa, and trabecular bone between 2–12 MPa [4].

Current bone tissue engineering approaches include cell based, scaffold based and delivery based strategies [5]. However, mechanical stability is still a major limitation of these scaffolds as tissue engineered

scaffolds thus far can only match the strength range of trabecular bone [6] making the implants unsuitable to withstand the patients' own weight without secondary fixation. Increasingly, scaffolds are being investigated for load bearing segmental bone defects [7]. However, few researchers have developed scaffolds that are stronger than trabecular bone and can be considered truly load bearing. Developing a load bearing scaffold is difficult because as the strength of the construct increases, the porosity and interconnectivity decrease dramatically [7].

The two factors that have received the most attention in tissue engineering are material composition and architecture of the scaffolds [8]. Throughout the last few decades different types of degradable scaffolds have been developed for bone using ceramics, polymers, and a combination of the two materials. Synthetic hydroxyapatite (HAp) has been used in the field of bone tissue engineering because of its biocompatibility, bioactivity [9–11] and its resemblance to the inorganic phase of natural bone [12]. β tricalcium phosphate (β TCP) is the second most used calcium phosphate material in bioengineering [13–17]. β TCP degrades much faster than HAp and it is also known for its excellent biocompatibility and osteoconductivity that stimulates the proliferation and differentiation of cells [14]. Because both materials are well suited for this application, scaffolds composed of a mixture of HAp and β TCP called biphasic CaP (BCaP) are commonly seen in the literature [18]. This combination is recognized for its osteoconductivity, bioactivity, biocompatibility and degradability [19]. BCaPs have a moderately controllable degradation rate [20] by changing the ratio of HAp to β TCP [20]. Basic material

* Corresponding author at: United States Army Institute for Surgical Research – Bldg 3611, Room 289-1; 3698 Chambers Pass, Fort Sam Houston, TX 78234-3877, USA. Tel.: +1 210 872 1675.

E-mail address: m_pilia@hotmail.com (M. Pilia).

Report Documentation Page

Form Approved
OMB No. 0704-0188

Public reporting burden for the collection of information is estimated to average 1 hour per response, including the time for reviewing instructions, searching existing data sources, gathering and maintaining the data needed, and completing and reviewing the collection of information. Send comments regarding this burden estimate or any other aspect of this collection of information, including suggestions for reducing this burden, to Washington Headquarters Services, Directorate for Information Operations and Reports, 1215 Jefferson Davis Highway, Suite 1204, Arlington VA 22202-4302. Respondents should be aware that notwithstanding any other provision of law, no person shall be subject to a penalty for failing to comply with a collection of information if it does not display a currently valid OMB control number.

1. REPORT DATE 01 FEB 2014		2. REPORT TYPE N/A		3. DATES COVERED -	
4. TITLE AND SUBTITLE Local Microarchitecture Affects Mechanical Properties of Deposited Extracellular Matrix for Osteonal Regeneration				5a. CONTRACT NUMBER	
				5b. GRANT NUMBER	
				5c. PROGRAM ELEMENT NUMBER	
6. AUTHOR(S) Pilia M., Pollot B. E., Agüero V., Appleford M. R.,				5d. PROJECT NUMBER	
				5e. TASK NUMBER	
				5f. WORK UNIT NUMBER	
7. PERFORMING ORGANIZATION NAME(S) AND ADDRESS(ES) United States Army Institute of Surgical Research, JBSA Fort Sam Houston, TX				8. PERFORMING ORGANIZATION REPORT NUMBER	
9. SPONSORING/MONITORING AGENCY NAME(S) AND ADDRESS(ES)				10. SPONSOR/MONITOR'S ACRONYM(S)	
				11. SPONSOR/MONITOR'S REPORT NUMBER(S)	
12. DISTRIBUTION/AVAILABILITY STATEMENT Approved for public release, distribution unlimited					
13. SUPPLEMENTARY NOTES					
14. ABSTRACT					
15. SUBJECT TERMS					
16. SECURITY CLASSIFICATION OF:			17. LIMITATION OF ABSTRACT UU	18. NUMBER OF PAGES 12	19a. NAME OF RESPONSIBLE PERSON
a. REPORT unclassified	b. ABSTRACT unclassified	c. THIS PAGE unclassified			

requirements for bone scaffolds are high porosity (60–99%) [19–28], an open interconnected architecture [29] and high permeability [30]. These factors play a role in determining the capacity of the scaffolds to provide high surface area and the ability to support blood vessel formation for the transport of nutrients. This has led to bone scaffolds with an architectural design that resembles trabecular bone [31], with high porosity, interconnectivity and fluid conductance. To date, cortical bone architecture is still a major challenge to recreate and remains virtually untested in the literature. Consequently, *in vitro* cortical bone like tissue development is also virtually unseen. Previous *in vivo* lamellar bone regeneration has been demonstrated [32], but no characterization at the micro level has been carried out to show similarity to native bone.

Osteons are continuously formed in bone as it remodels through time or after injuries. First, osteoclasts resorb the old/damaged bone, leaving behind small microchannels that are closely followed by a continuous supply of osteoblasts that are being delivered to the remodeling area by blood capillaries and fluid movements (Fig. 1). Once the osteoblasts attach to the walls of the resorbed area they start secreting and mineralizing ECM, until they become entrapped in their own matrix and differentiate into osteocytes [33]. Thus, native formation and remodeling of osteons present the microchannel like architecture as a template for potential biomimetic osteonal regeneration.

In this study we recreated the microarchitecture of cortical bone with osteonal microchannels with the goal to investigate cortical bone like growth *in vitro*. A 3D scaffold with longitudinal microchannels spanning the entire length of the construct was developed using two different materials: BCaP and HAp. Subsequently the osteoblast response to the microchannel architecture was investigated using human fetal osteoblasts (HFOB) with single or multiple seedings over

the course of a 24 day *in vitro* study. It was hypothesized that the artificial microchannels will mimic an osteonal model that will serve as a scaffold for bone like ECM deposition of a lamellar structure with a specific cellular orientation and organization. This was the first attempt at recreating a cortical bone like environment for osteoblasts to populate and form organized osteonal structures *in vitro* in 3D.

2. Materials and methods

2.1. Fabrication of the CaP scaffolds

Custom designed molds used to create the CaP scaffolds consisted of three different parts: a cement cylinder and two holed stainless steel plates. Dental stone cement (Coecal™ Type III Dental Stone GC America Inc, Alsip, IL) was mixed with distilled water (3:1 w/v ratio) and shaped into a cylinder of 20 mm diameter. Subsequently a hole (diameter 10 mm) was drilled in the center to form molds into which CaP slurry was cast. Each cement mold measured 20 mm in height. At each end of the cement molds two stainless steel plates, 2 mm thick were attached. Each of these plates were manufactured using small hole electrical discharge machining (EDM). Each plate was patterned with 136 holes, each of 700 μm diameter. Fig. 2A–C shows the mold assembly. Once assembled, 26 gauge stainless steel needles (diameter 500 μm) (McMaster Carr, Atlanta GA) were passed through both metal plates and were left in place for the casting to serve as the negative templates for microchannels.

The CaP scaffolds were made by solution casting. Two sets of scaffolds were made using HAp and 60:40 HAp:β-TCP mixture (BCaP). The nano synthetic CaPs were purchased from OssGen, South Korea. A liquid suspension for each combination of materials was created following a previously described method [34]. Briefly, the binders used to stabilize the suspension structure included 3% high molecular weight polyvinyl alcohol, 1% v/v carboxymethylcellulose, 1% v/v ammonium polyacrylate dispersant, and 3% v/v N,N dimethylformamide drying agent. The solution was then cast into the constructed molds and sintered in a high temperature furnace (Thermolyne, Dubuque, IA). The sintering process profile contained a ramp increase in temperature of 5 °C/min up to 300 °C with a hold time of 1 h, then up at the same rate to 600 °C for 1 hour hold, and finally to 1230 °C for a 5 hour hold. The sintered disks were then cooled at a rate of 5 °C/min until room temperature was achieved. Within each material type, the microchannels were created using SS needles. As a result, a total of 2 groups were used for scaffold characterization. Detailed scaffold construction technique is shown in Fig. 2D–G.

2.2. Scaffold characterization

2.2.1. Mechanical testing

Compressive strength, elastic modulus and toughness of the scaffolds were measured in this study. Using a sample size of 12 per material, cylindrical scaffolds (14 mm in length and 7 mm in diameter) were prepared in order to conform to the 2:1 aspect ratio specified in the ASTM D695 compression testing standard. Prior to testing, polymer sheet end caps were used with all scaffolds to minimize edge artifacts, and scaffolds were equilibrated to 37 °C in distilled water for 12 h prior to testing. Mechanical testing of the scaffolds was performed in a hydrated state on an Insight 5 test frame (MTS, Eden Prairie, MN) in displacement control mode at a constant strain rate of 1.25 mm/min.

2.2.2. Porosity measurement

Porosity and material density measurements were obtained using 12 samples per group from the solid volume fraction of the scaffold. True solid volumes of the scaffolds were measured using helium pycnometry (AccuPyc 1340, Micromeritics, Norcross, GA). The length and diameter of each scaffold were measured by averaging across three independent measurements to calculate the volume of the

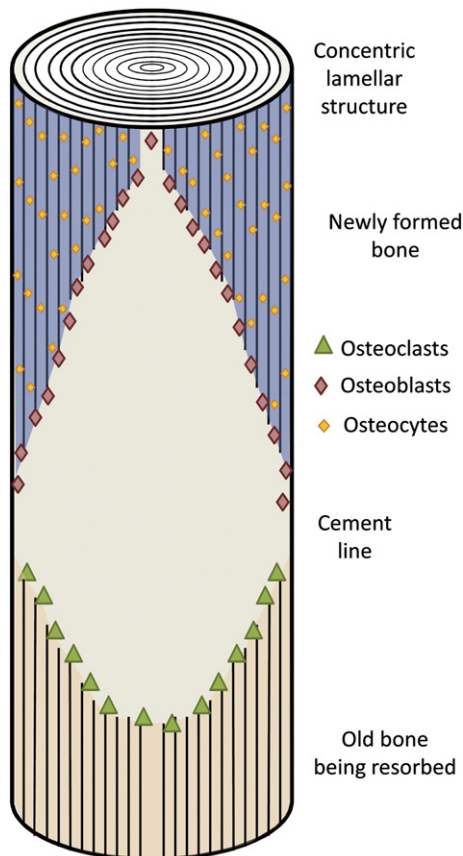


Fig. 1. Schematic representing bone remodeling. This is the process during which osteons are formed. Osteoclasts resorb the old/damaged bone followed by the osteoblasts that attach to the cement line and grow from the outside in. As osteoblasts become trapped in their own matrix, they differentiate into osteocytes.

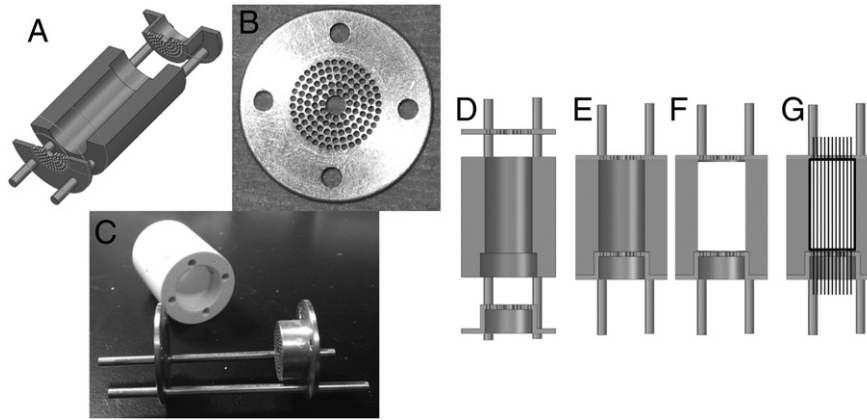


Fig. 2. Cross section e-drawing (A) of the molds used to create the cortical scaffolds. Each mold was made of a cement block (C) and two metal plates with 136 holes (B). D–G – Step-process used to create the cortical scaffolds. (D) First, the molds were assembled with the 3 pieces: the cement block (middle), and the two metal plates. (E) The metal plates were lowered into the cement mold where (F) the CaP slurry was injected. (G) Only at this point were the SS needles passed through the holes of each metal plate. After the samples were lyophilized the needles were removed and the scaffolds were sintered.

scaffolds. Each sample was weighed using a microbalance (AB 135 S/FACT, Mettler Toledo). This allowed the computation of the porosity as the void volume fraction and material density as the ratio of scaffold mass to solid volume.

2.2.3. Micro computed tomography (μ CT) analysis

Twelve scaffolds per group were scanned using micro computed tomography (micro CT) SkyScan 1076 (Skyscan, Aartselaar, Belgium) at 8.87 μ m spatial resolution. The reconstruction thresholds were chosen such that the reconstructed scaffold volume using Mimics (Materialise, Leuven, Belgium) matched the volume measured using helium pycnometry. Morphometric analysis was carried out on CT images using CTAnalyzer vs.1.4 (Skyscan). In order to determine channel organization, histomorphometric parameters were computed for each of the scaffolds over the total 3D volume of the scaffold. The parameters computed were scaffold volume ratio (SV/TV), scaffold surface density (SS/SV), inter channel thickness (Ch. Sp.), and channel diameter (Ch. Th.).

2.2.4. Permeability testing

Scaffold permeability was measured using a custom flow apparatus consisting of a fluid reservoir that fed into a sample chamber and opened to the atmosphere. The pressure head was thus equal to the height of the liquid column above the sample chamber. Using Darcy's Law, permeability is defined as:

$$k = \frac{m\mu L}{A_{cs}\rho\Delta P} \quad (1)$$

where k is the permeability (m^2), m is the mass flow rate, μ is the fluid viscosity, L is the scaffold length, A_{cs} is the mean cross sectional area, ρ is the fluid density and ΔP is the pressure drop across the scaffold. A sample size of 12 scaffolds per group was used for permeability measurement and permeability was measured in triplicate for each scaffold. Distilled water was used for permeability measurement, with all scaffolds allowed to equilibrate by repeatedly running water through the scaffolds for 5 min prior to testing. Permeability was then computed by measuring the volume of water collected over four different lengths of time through the scaffold.

2.2.5. Material degradation profile

Scaffold degradation was investigated through calcium (Ca^{2+}) release in both neutral (pH = 7.4) and acidic (pH = 6.0) phosphate buffered solution (PBS) to recreate physiological wound healing conditions [35]. Acidic PBS was made by slowly adding 1 M HCl while continuously stirring the solution to reach a pH of 6.0. Cross sections of the scaffolds were used to test Ca^{2+} release in each group ($n = 8$).

Each section was 2 mm thick and was made using a microtome saw (SP1600, Leica; Wetzlar, Germany). The samples were placed in a 48 well plate and immersed in 1 mL of PBS (neutral or acidic). Ca^{2+} released in the PBS was measured at day 1, 3, 5, and 7. Ca^{2+} release was measured using a quantitative calcium reagent kit (Pointe Scientific, Inc. Canton, MI). Specifically, 10 μ L of sample PBS solution was added, to 990 μ L of reagent solution. After 5 minute incubation, the calcium in solution was determined using a plate reader (Biotek Synergy 2 Winooski, VT) by absorbance measurement at 570 nm with comparison to an environmental calcium standard control.

2.3. In vitro human fetal osteoblast cell culture study

Investigation of *in vitro* osteon development was conducted in 2 mm thick cross sections of the HAp and the BCaP scaffolds. The scaffolds were sectioned using a microtome saw (Leica SP1600; Wetzlar, Germany). The samples were then sonicated in 70% ethanol and sterilized by ethylene oxide (AN74i Anprolene gas sterilizer, Andersen Sterilizers, Inc) for a 12 hour cycle.

Human fetal osteoblasts (HFObs) (Cat. # 406 05f, Cell Applications, Inc.) were used to evaluate osteon formation in the newly developed scaffolds. The cells were cultured in growth media containing Dubecco Modified Eagle Medium (DMEM), 10% Fetal Bovine Serum (FBS), and 1% Penicillin Streptomycin Amphotericin B Solution (PSA) (all purchased from Invitrogen, USA). When cells reached confluence on the cell culture flask, the HFObs were washed with phosphate buffered saline (PBS) and then 0.25% Trypsin/EDTA was added in osteogenic induction media (DMEM, 3% FBS, 1% PSA, 10 mM Glycerolphosphate, 50 μ g/mL Ascorbic acid and 10nM Dexamethasone). The cells in solution were counted (Z_2 Coulter® Particle Count and Size Analyzer; Beckman Coulter™ Brea, CA) and seeded on the disks at a density of 55,000 cells/cm². Four time points were tested: 6, 12, 18 and 24 days ($n = 6$). At the end of each time point the samples were washed in PBS and fixed in 4% formaldehyde. Osteogenic induction media used in this study stimulates bone precursor cells to differentiate into osteoblasts, allowing ECM deposition and mineralization, but limited proliferation. When attempting to grow an osteonal structure *in vitro*, it is necessary to recreate the continuous delivery of cells as it occurs *in vivo*. Therefore, multiple seedings every 3 days were performed on each scaffold, so that new undifferentiated cells could attach to the cellular wall and mature into osteoblasts.

2.4. Mechanical ECM characterization of the artificial osteons

Representative disks from each investigated group were tested to determine the mechanical properties of the cell's ECM depositions.

The cells on the surface of the disks were gradually dehydrated in ethanol to preserve cellular structure. Specifically, the disks were moved into a 20/80 (vol/vol) ethanol in water for 4 h, then 40/60, 60/40, 80/20, and 100% ethanol two more times for the same duration. The disks were then epoxied onto a 3 cm diameter metal cylinder using a very thin layer of epoxy glue. Using a commercial nano indenter (MTS nano indenter XP, MTS System Corporation, MN), the reduced elastic modulus (E_r) and the microhardness (H) of the deposited ECM were determined. Before measuring each group the nano indenter location was calibrated using a 5 indent template. The indenter's microscope objective ($20\times$) was then used to find the cell layers along the perimeter of the microchannels. For each experimental group the indents were made within the edges of the microchannels where cell growth was seen. The indents were performed using a Berkovich tip and a standard trapezoidal loading profile with a loading rate of 250 $\mu\text{N/s}$ until a maximum load of 500 μN was applied [36]. E_r and H were determined using a previously described method [37]. Briefly, the Young's modulus for the tested material (E_m) was calculated by assuming that the cells had a Poisson's ratio (ν_m) of 0.3. For the diamond indenter the Young's modulus (E_i) was set to 1140 GPa, with a Poisson's ratio (ν_i) of 0.07. Eq. (2) was used to calculate E_m [37]. Hardness instead was calculated using Eq. (3).

$$E_m = \frac{1 - \nu_m^2}{\frac{1}{E_r} - \frac{1 - \nu_i^2}{E_i}} \quad (2)$$

$$H = \frac{P_{\max}}{A} = \frac{P_{\max}}{F(h_c)} \quad (3)$$

in which P_{\max} is the peak load and A is the projected area of contact at peak load evaluated by a function which relates the cross sectional area of the indenter to the vertical distance from its tip (h_c) [37].

The modulus and hardness readings that fell into the control HAP readings \pm standard deviation were discarded where the indent was measuring the actual CaP layer and not the cell ECM. A total of 100 random tests were performed from each disk.

2.5. *In vitro* osteoid development and cell orientation characterization

After being fixed in 4% formaldehyde, 2 disks per group were analyzed for osteoid development within 10 random microchannels. Each sample was analyzed using a light microscope at $10\times$ magnification. Using the software Bioquant Osteo system (Bioquant Osteo 2010, Nashville, TN), the original microchannel area and perimeter were found, as well as the osteone area and thickness. In the instance that the osteoid

bridged across the microchannels, the width of the cell growth was averaged between the bridge fibers and the structure along the perimeter of the microchannels, giving false negative measurements of osteoid secretion thickness. Fig. 3 is a graphical depiction of the osteoid formation and its analysis.

A total of 20 random microchannels per group were used for cell orientation analysis. The disks were first washed in PBS, following which the cell membrane was permeabilized in 0.1% Triton X 100 in PBS (PBS T) for 1 h. The samples were washed again in PBS and sectioned in two halves to expose the inner longitudinal walls of the microchannels. The two halves were placed back on the well and a drop of ProLong® Gold Antifade with DAPI was added. After a 12 hour incubation at 4 °C with the DAPI stain, the disks were analyzed under fluorescent microscope (SFL7000, Leica) for nucleus orientation. Twenty random images were taken throughout the disks from inside the artificial microchannels. Because the disks had cells growing on a three dimensional substrate, the quantification of the cells was performed on the valley of the microchannels. The DAPI stained nuclei were used to determine the angle of orientation of the cells with respect to the microchannel direction. This was done assuming that when the nucleus of the cell was elliptical in shape, the long axis of the nucleus matched the long axis of the cytoskeleton of the cell [38]. Cells undergoing mitosis were not measured for alignment. Images were analyzed using Bioquant Osteo system (Bioquant Osteo 2010, Nashville, TN). The angle of the cell was measured in degrees, with 0° being parallel to the microchannel direction, and 1 to 90° and 1 to -90° being of an angle to the right or to the left of the microchannel respectively. A schematic to describe this quantification is shown in Fig. 3.

2.6. Statistical analysis

All data were reported as average \pm standard error. The statistical test used to analyze the data was a two way analysis of variance, and Tukey's comparison test was used to determine statistical significance between individual groups. All statistical tests were performed using SigmaPlot® (version 11.0, Systat Software, Inc.). Differences were considered significant at $p < 0.05$. The difference between variances of distribution was evaluated using an F Test (MedCalc® V 12.2.1.0).

3. Results

3.1. Scaffold characterization

3.1.1. Mechanical testing

Compressive strength, modulus and toughness were determined with compressive testing (Fig. 4A C). A total of 2 scaffold materials were tested (HAP, BCaP). No significant difference was seen in the

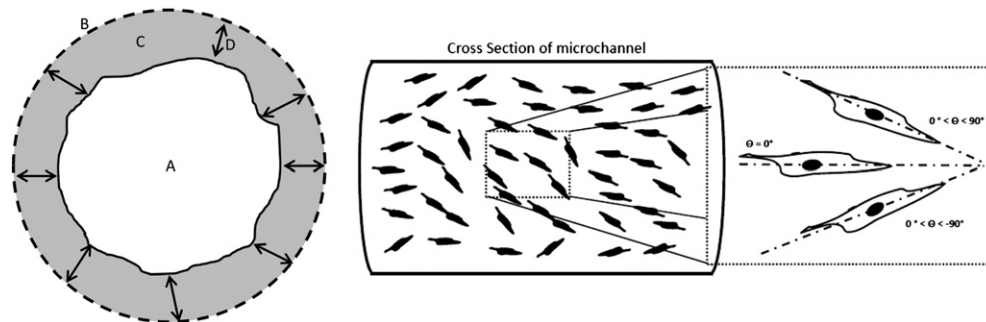


Fig. 3. (left) Drawing depicting the measurements performed in the *in vitro* osteoid secretion. The area (A) and perimeter (dotted line - B) of the microchannel were measured, then the area of the osteoid secretion (grayed area, C), and last the average osteoid width (D). (Right) Graphical representation of the technique used to measure the orientation of the cells growing in the flat control HAP disks. Particular attention was paid to avoid bias orientation due to the meniscus effect due to the media on the well plate wall during cell culture. This was accomplished by measuring the cells from top to bottom and from left to right. When the long axis of the cell nuclei was parallel to the direction of the microchannels the angle was set to 0°. All the cells that were angled to the right were measured anywhere between 0 and 90°, whereas the cells angled to the left were measured with a negative number, 0 to -90°.

compressive strength between any of the groups. Statistically, the material and the construction technique had no effect on the maximal strength. The primary mode of failure observed in all samples tested was initial longitudinal cracking along the surface layer of the scaffold resulting in the formation of slender beams and followed by secondary crack propagation in the scaffold interior. Final structural collapse was observed following failure of the slender surface beams in flexure and progressive crushing of the interior porous structure.

The compressive modulus was also calculated from the compressive testing as the slope of the initial linear region of the stress–strain curve. The results did not show any differences between the HAp scaffolds and the BCaP constructs. Similarly, the compressive strength did not demonstrate significant difference.

The last value analyzed from the mechanical testing was toughness. This was calculated as the area under the stress–strain curve to failure (defined as ability to carry <20% of peak load). It was observed during testing that the post yield stress levels at which further crack propagation occurred in the microchannel were high. No significant differences were seen between the materials used to create the microchannels.

3.1.2. Architectural characterization

Porosity measurements were obtained by solid volume fraction technique. Data consistently demonstrated that the method used to recreate the microchannels in the scaffolds had a significant effect on the porosity of the HAp ($p = 0.004$) and BCaP ($p = 0.003$) scaffolds. The different CaP materials had no influence on porosity, and no specific trend was observed. Table 1 shows the detailed results.

No significant differences were observed in scaffold surface density between the experimental groups, indicating that the available surface area for cellular attachment was similar in all groups (Table 1). No

significant differences were observed within the 2 groups tested in terms of channel thickness (Ch. Th., diameter of the channels) based on the type of calcium phosphate used. This result demonstrated that the channel sizes were all comparable within the manufacturing process and allows for a direct comparison between groups of *in vitro* cell response.

Density measurements were determined from using helium pycnometry and weight measurements (Table 1). Unlike the porosity readings, the microchannel fabrication material had no significant impact on density. A significant difference was expectedly seen between the different CaP materials used to create the scaffolds. The HAp constructs had significantly higher density than the BCaP group ($p < 0.001$).

3.1.3. Permeability testing

Permeability testing was conducted on the different scaffolds (Fig. 4D). The material used to create the scaffolds had no significant difference, though a trend was seen in which the BCaP group had higher porosity than the HAp.

3.1.4. Material degradation profile

The calcium released from each sample group was determined for 7 days, until linear release was seen. The samples submerged in the 6.0 pH solution showed higher release than the samples submerged in the neutral pH PBS. Within the wound pH testing, the Ca^{2+} released from the HAp was determined to be statistically lower than the BCaP group starting from the day 2 reading ($p < 0.001$). Within the physiological testing, no significant changes between the materials' Ca^{2+} released was seen. Fig. 5 shows the results.

Since both HAp and BCaP had reached linear degradation profile after day 1 ($R^2 = 0.969$) the cumulative Ca^{2+} levels for day 24 were

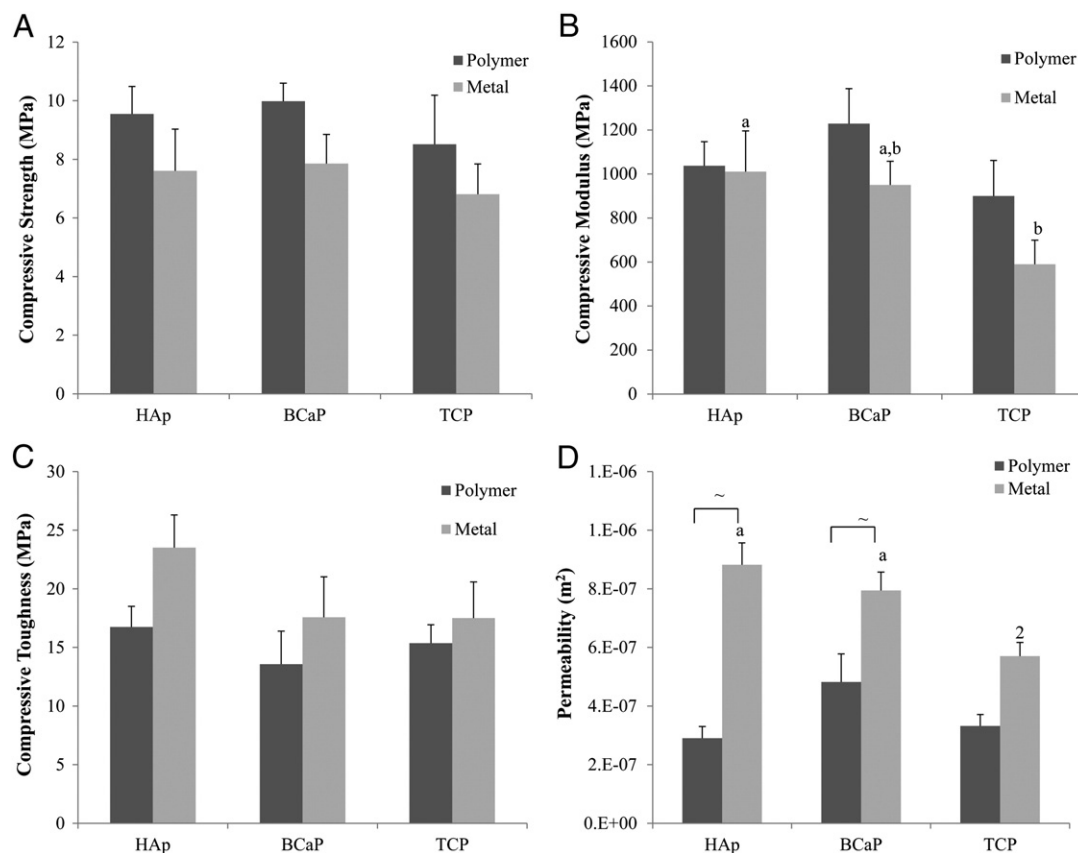


Fig. 4. Histograms representing (A) compressive strength, (B) compressive modulus, and (C) compressive toughness. Compression testing was performed on scaffolds built of two different materials: HAp and BCaP. Each group of scaffolds had microchannels built with stainless steel needles. $n = 12$ for each group. (D) Permeability results show no significant differences between the HAp and BCaP scaffolds. No significant differences seen between any of the groups. All data shown as mean \pm standard error.

Table 1

Architecture characterization of calcium phosphate scaffolds determined by helium pycnometry and microCT. (SS/SV – scaffold surface density, Ch. Sp. – inter-channel spacing, Ch. Th. – channel thickness or diameter). Superscript letters indicate the statistical differences between the CaP materials.

	HAp		HAp-TCP		TCP		
	PU	SS	PU	SS	PU	SS	
Porosity	21.0 ± 1.6 ^{1*}	31.0 ± 1.1 [*]	26.8 ± 1.8 ^{2^}	33.2 ± 0.4 [^]	20.0 ± 1.3 ^{1#}	31.8 ± 1.8 [#]	%
SS/SV	5.46 ± 0.3	6.63 ± 0.2	6.57 ± 0.3	7.86 ± 0.2	5.44 ± 0.3	7.66 ± 0.7	1/mm
Ch. Sp.	539 ± 18 [*]	420 ± 16 [*]	462 ± 17 [^]	384 ± 5 [^]	533 ± 15 [#]	400 ± 21 [#]	μm
Ch. Th.	307 ± 23	377 ± 20	377 ± 39	363 ± 3	296 ± 39	335 ± 8	μm
Density	3.180 ± 0.00 ¹	3.174 ± 0.01 ^a	3.142 ± 0.01 ²	3.136 ± 0.00 ^b	3.133 ± 0.01 ²	3.117 ± 0.00 ^b	mg/cm ³

calculated and demonstrated the overall amounts of Ca²⁺ potentially available for cell induced mineralization.

3.2. *In vitro* osteoid development and cell orientation characterization

Cell orientation within the walls of the artificial microchannels was assessed from nuclei orientation with regards to the microchannel length. The individual materials and the individual types of seeding were also investigated over the length of the study to determine the role of these factors in cell orientation. These findings are shown in Fig. 6. At day 24 both the seeding type and the scaffold material played no role in cellular organization (Fig. 7).

In vitro osteoid formation was evaluated throughout 24 days in the developed scaffolds. A total of four measurements were used to quantify osteoid development within each microchannel (osteon). The first parameter measured was the area of the new osteoid formation normalized by the area of the original microchannel to account for slight changes. The results showed that from day 12 to 24 the number of cell seedings made a significant difference in the volume of the osteoid deposited ($p < 0.001$) both within the HAp scaffolds and the BCaP scaffolds. In the HAp scaffolds, time showed significant differences both within the single and the multiple seedings. The single seedings (Fig. 8A) demonstrated significant differences between day 18 and 24 ($p = 0.002$) and between days 24 and 12 ($p = 0.008$). Within the multiple seedings, significant differences were seen between days 6 and 12,

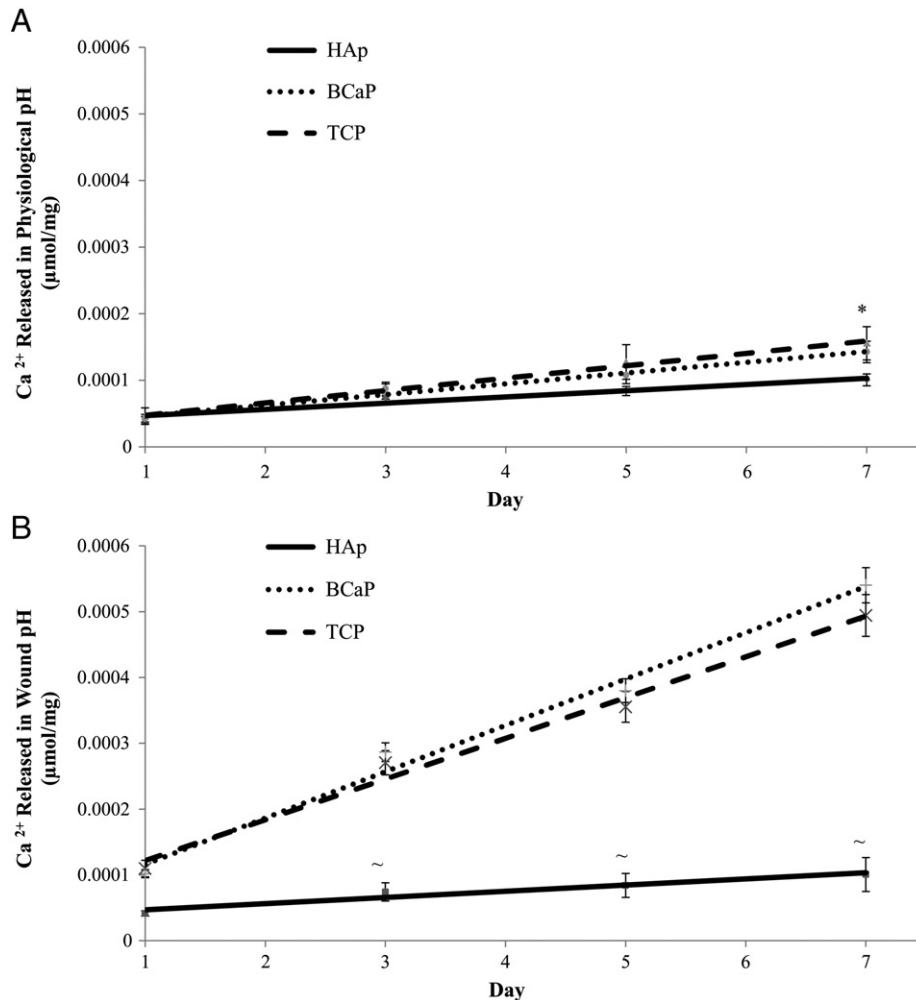


Fig. 5. Histograms showing the cumulative Ca²⁺ released curves for the two materials used to create the scaffolds: HAp and BCaP. A) Ca²⁺ released in the wound pH (6.0); B) The Ca²⁺ released in the physiological environment reaches linear release after day 2 (R^2 – HAp:0.9845; BCaP: 0.9877). $n = 8$ for each group. All data shown as mean ± standard error. * $p < 0.05$; ~ $p < 0.001$.

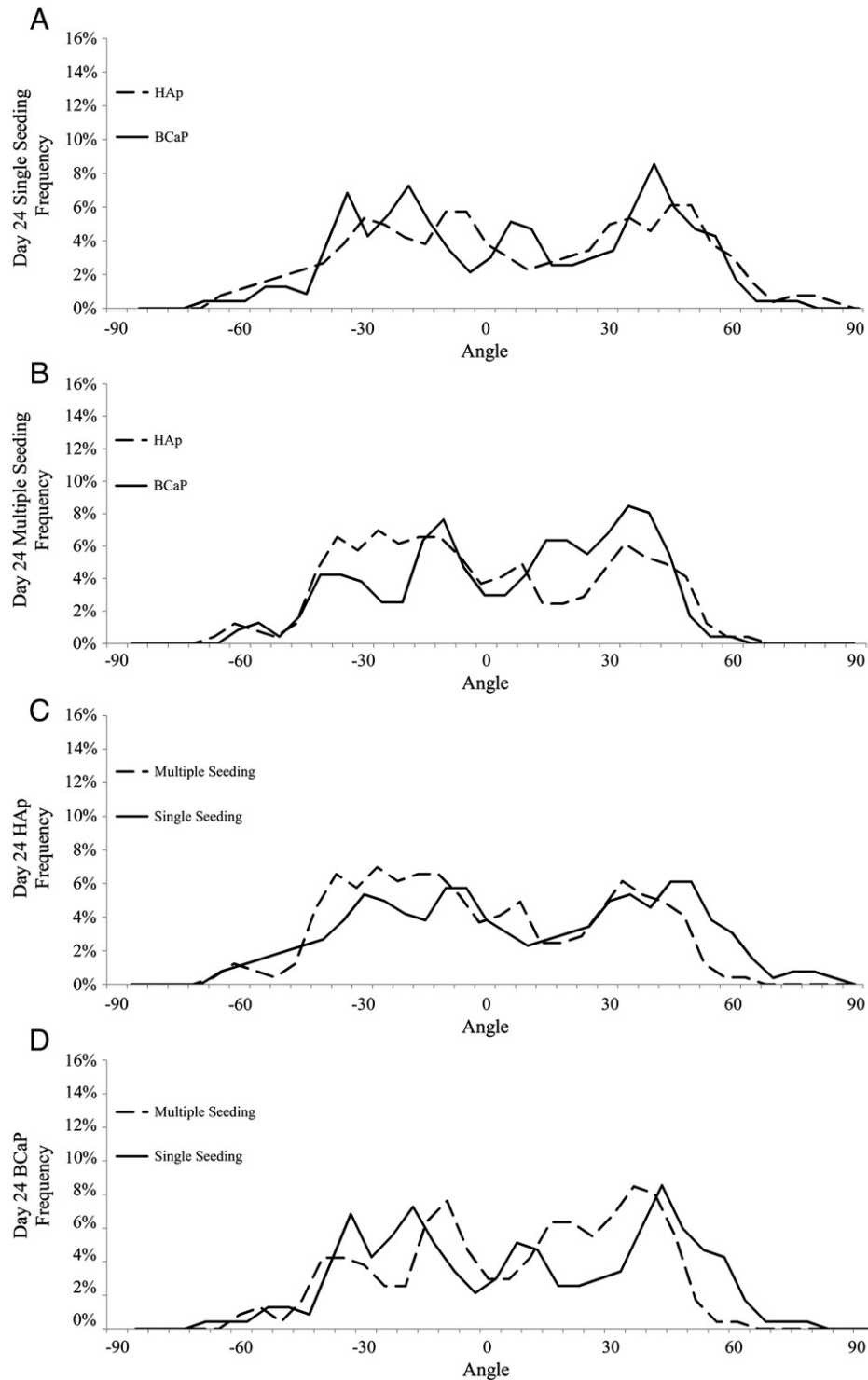


Fig. 6. Role of seeding and scaffold material on cellular organization. The narrower and the higher the frequency curve was, the higher the organization of the cells. A) The progress of the HAp scaffolds with single seeding over time. Significant differences between the variances were seen between day 6 and 12 ($p < 0.001$) and between day 6 and 18 ($p = 0.001$). B) shows the change in cell organization of the HAp scaffold with multiple seeding over the 24 days. Significant differences were seen between day 6 and 12 ($p < 0.001$), 18 ($p < 0.001$) and 24 ($p = 0.003$). (C) shows the progress of the BCaP scaffolds with the single seeding over time. Significant differences were seen between day 6 and 12 ($p = 0.036$) and 18 ($p < 0.001$). On the bottom right (D) are shown the changes in cell organization of the BCaP scaffolds with multiple seedings. No significant differences were seen in the curve variances (F-Test).

18, 24 ($p < 0.001$), and between days 12 and 24 ($p = 0.018$). The area of the osteoid formation amongst the BCaP scaffolds (Fig. 8B) was influenced by time. Specifically, when analyzing within the single seedings, significant differences were seen between days 6 and 18 ($p = 0.001$) and between days 6 and 24 ($p = 0.042$). More significant differences were seen within the multiple seedings groups, and specifically between days 6 and all other days ($p > 0.005$).

The second parameter measured was the average width of the new osteoid deposition, reported as % osteoid bridging. When analyzing the HAp scaffolds, (Fig. 8C) a few significant differences between the seedings were seen. At all four time points the multiple seeding groups demonstrated significantly higher osteoid width than the single seeding groups ($p > 0.001$). Further significant differences were seen within the multiple seeding groups across time. Specifically, day 6 was different

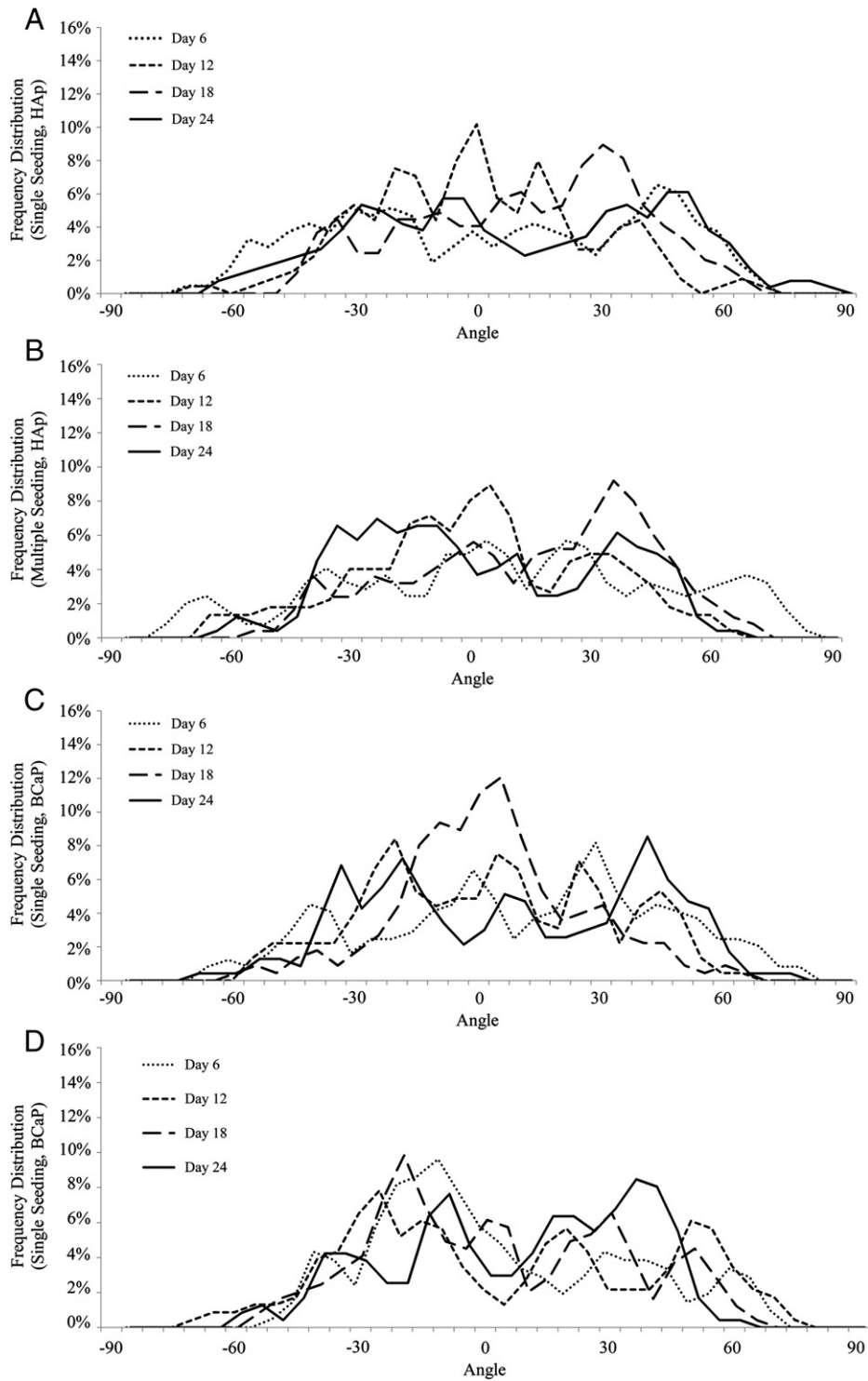


Fig. 7. Frequency graph of the cellular organization at day 24 for the single seedings (A) and for the multiple seedings (B). The narrower and the higher the frequency curve was, the higher the organization of the cells. No significant differences were seen in the curves. Statistical significance was analyzed between variances using an F-Test. Frequency graph of the cellular organization at day 24 for the HAp group (C) and for the BCaP group (D). The narrower and the higher the frequency curve was, the higher the organization of the cells. No significant differences were seen in the curves. Statistical significance was analyzed between variances using an F-Test.

from days 12, 18 and 24 ($p < 0.001$). Day 12 was different from day 24 ($p < 0.001$). The same differences were seen in BCaP scaffolds (Fig. 8D), where day 6 was different from day 12, 18 and 24 ($p = 0.003$). Fig. 9 shows the osteoid formed within the HAp (Fig. 9A B) and the BCaP (Fig. 9C D) microchannels over a 24 day period (Fig. 9 left to right). The difference between the single (Fig. 9A C) and the multiple (Fig. 9B D) cell seedings can also be seen.

3.3. *In vitro* mechanical ECM characterization of the artificial osteons

In vitro cell culture was performed only on (HAp and BCaP), and each material had been seeded either only one time (single seeding) or every 3 days (multiple seeding) for the duration of the study. β TCP was not used because of the high clinical levels of Ca^{2+} released *in vivo*. Hardness and modulus of the newly deposited ECM around the walls of the

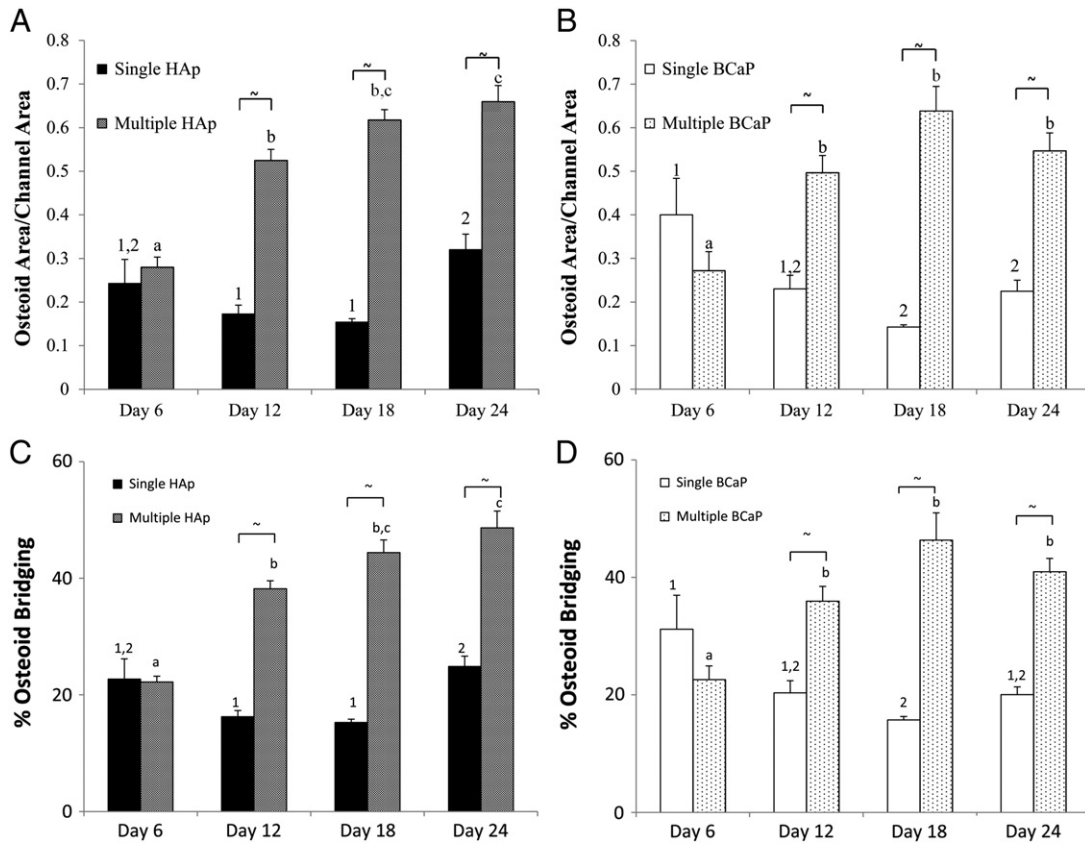


Fig. 8. Histograms showing the results of the *in vitro* osteoid characterization. A) shows the osteoid area within the HAp scaffolds. Multiple seedings were helpful in increasing the osteoid area at days 12, 18 and 24. Time also had a significant effect on osteoid secretion in both the multiple and the single seedings. B) shows the osteoid secretion within the BCaP scaffolds. As in the HAp groups, multiple seedings had a positive effect on osteoid secretion at days 12, 18 and 24. Time also had a significant effect on the osteoid secretion. The multiple seeding groups increased in size from day 6 on, whereas the single seedings demonstrated a decrease in area from day 12 on. All data shown as mean \pm standard error. $\sim p < 0.001$.

artificially created microchannels was assessed in this study using a nano indenter. The test was performed at day 24 from 50 random microchannels. The hardness values show that cell seeding did not play a significant role in the hardness of the ECM. However, a significant difference in ECM hardness was seen between the different material groups used to build the scaffolds. The ECM deposited on the HAp scaffold had significantly lower hardness values than that of the BCaP. This was valid for both the single ($p = 0.014$) and the multiple ($p = 0.035$) seeding groups. The higher hardness value was seen in the BCaP single seeding with 1.94 GPa, whereas the lowest value was 0.78 GPa in the HAp, multiple seeding group. Modulus measurements ranged between 25.23 and 18.69 GPa, which corresponded to the BCaP multiple seeding and the HAp single seeding respectively. No statistical significance was seen between the samples, which indicate that neither the material nor the number of seedings had an effect on ECM moduli. However, a trend was observed in which the ECM deposited in the BCaP scaffolds had higher moduli values. Fig. 10 shows these results. The value of the ratio of BCaP hardness to HAp hardness was found to be 2.42 for the single group and 2.27 for the multiple groups.

4. Discussion

Most bone tissue engineered scaffolds currently being investigated resemble the architecture of trabecular bone, with large, interconnected pores [15]. The purpose of this research was to develop a 3 D bone like architecture that mimics cortical bone rather than trabecular bone. This was the first time this type of scaffold architecture was built, and replicating osteon like microchannels in CaP materials was quite challenging. The ability to recreate *in vitro* osteonal formation is important as it can be potentially used to create a tissue engineered scaffold to recreate mechanically sound cortical bone rather than disorganized woven bone.

Two different materials were used to construct the scaffolds: HAp and BCaP (a 60:40 w/w mixture of HAp and β TCP). This combination of calcium phosphate materials has been previously attempted and has reported strong biocompatibility and active surfaces [19] as well as acceptable resorption rates that match bone formation [20]. Stainless steel needles were used to mold the microchannels during scaffold fabrication in an attempt to recreate the artificial osteon templates. These needles were rigid, and μ CT characterization showed no interconnectivity between neighboring channels as they were very uniform and precise throughout the scaffold length. Direct cellular interaction with the biomaterial required precise channels with high permeability to support cellular growth, and the ss needles used as porogens in the scaffolds were appropriate for fabrication. However, naturally occurring osteons and Haversian systems do have interconnections (Volkmann's canal) and thus it would be of great interest in the future to develop in interconnectivity between the microchannels.

Calcium release was investigated on our scaffolds by submersion in PBS solution for 7 days. Normally calcium release is studied in neutral pH conditions ($pH = 7.4$). However, during trauma and in wound healing conditions, this pH is dramatically reduced anywhere between 5.5 and 6.5. This occurs as a defense response to local inflammatory responses and possible infections [35]. Thus, to determine a more accurate calcium release curve of the materials, and to ensure that toxic levels of Ca^{2+} were not present, the degradation profile in wound healing acidity ($pH = 6.0$) was also determined. Not surprisingly, the acidic conditions significantly increased the amount of Ca^{2+} released in both construct formulations. It was determined that even the highest levels of Ca^{2+} released during degradation were lower than the physiologically toxic levels of Ca^{2+} in the body (10 mmol) [39]. Degradation profiles of CaP materials have been previously reported [40]; unfortunately the differences between all the CaP powders available, and the manufacturing

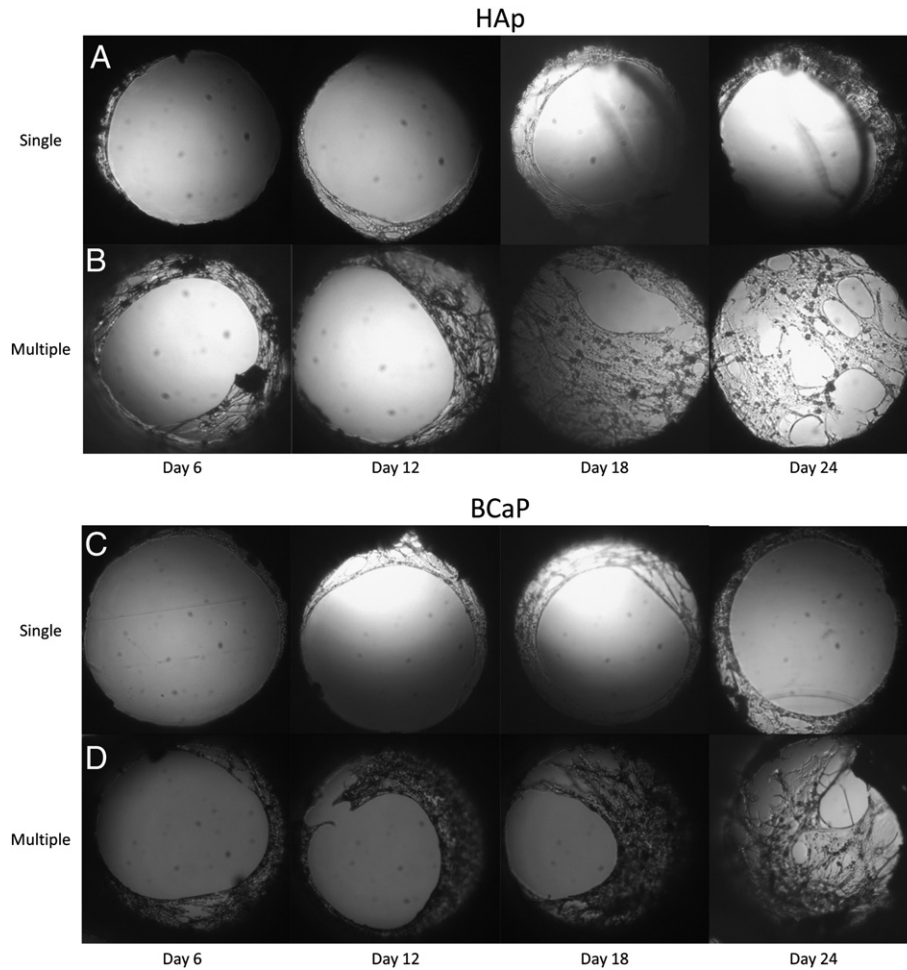


Fig. 9. Brightfield microscopy (100× magnification) photographs of the osteoid secretion inside the microchannels. (A,C) osteoid secretion inside the HAp (A) and BCaP (C) microchannels at 6, 12, 18, and 24 days (left to right). Because only a single cell seeding was performed at day 0, and because the cells were cultured in osteogenic media, no proliferation was seen and the osteoid area remained unchanged. (B, D) osteoid secretion in the HAp (B) and BCaP (D) microchannels during 6, 12, 18, and 24 days (left to right). These scaffolds received multiple cell seedings every 3 days and thus the increase in osteoid secretion was seen over time. Notice at day 24 that the secretion forms bridges within the microchannel, which account for the sudden decrease in osteoid-secretion thickness while maintaining high surface area measurement.

and sintering processes used by researchers have rendered it infeasible to compare all the different scaffolds in the literature [41–46].

To evaluate the mechanical properties of the scaffolds and to demonstrate their ability to possibly function as load bearing constructs, compressive testing was required. Three different measurements were

determined: the compressive strength, modulus and toughness. The compression strength recorded in this study varied from 3.3 to 18.7 MPa, with an average of 8.4 ± 4.05 MPa. Comparatively, the compression strength of cortical bone is in the range of 100–230 MPa⁴, which is an order of magnitude higher than our recorded values. The

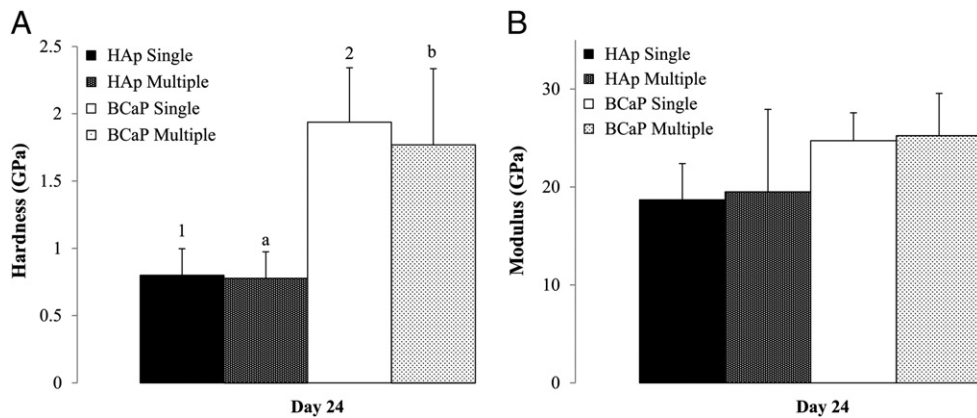


Fig. 10. Micro-hardness (A) and reduced modulus (B) of the freshly deposited ECM in the artificial osteon. The readings were performed after 24 days of *in vitro* HFoB culture in 2 mm thick sections of the scaffolds. The material used for the constructs were HAp and BCaP. Different numbers of cell seedings were investigated: single initial and multiple seedings every 3 days. A) ECM hardness shows that the material with which the scaffolds were constructed had a significant effect on the ECM deposition ($p < 0.05$). B) No significant differences were seen in the modulus values at day 24, only a visible trend was observed in which the BCaP scaffolds had higher moduli than the HAp groups. All data shown as mean \pm standard error.

compressive strength of trabecular bone instead ranges between 2 and 12 MPa⁴. It should be considered that while the porosity of natural trabecular bone and cortical bone are 30–90% and 5–13% respectively [4], the porosity for the scaffolds used in this study was $59.8 \pm 7.7\%$ which is more similar to dense trabecular bone than cortical bone. Thus the scaffold design, though architecturally similar to native cortical bone, showed biomechanical characteristics similar to that of dense trabecular bone. What remains to be determined is whether this kind of architecture will gain strength *in vivo* when the microchannels are filled with cells and ECM. Throughout these results there were no significant differences between the HAp and BCaP used to build the scaffolds and there were no clear trends that favor one material over another.

The different scaffold materials had overall porosities that ranged between 61.6 (HAp) and 65.2% (BCaP). Tissue engineered scaffold requirements for porosity are between 60 and 99% [19–28]. When analyzing the density results, the type of CaP used played a significant role. The HAp group was far denser than BCaP group. The material density for HAp was 3.17 ± 0.01 . This compares well with the absolute material density of HAp (3.1) [4].

Permeability testing performed on the scaffolds demonstrated significantly high fluid flow through both the HAp and BCaP groups with practically no differences in between. This result was due to very similar sample geometry. Permeability, or fluid conductance, has been indicated by Hui et al. as the only way to predict *in vivo* success. In the same study threshold conductance was determined to be $1.5 \times 10^{-10} \text{m}^3 \text{s}^{-1} \text{Pa}^{-1}$ [30]. In our experiments, the permeability values ranged between $8.82 \times 10^{-7} \text{m}^2$ and $2.90 \times 10^{-7} \text{m}^2$, and the conductance values ranged from 6.9×10^{-10} to $2.1 \times 10^{-9} \text{m}^3 \text{s}^{-1} \text{Pa}^{-1}$, values which were 4 to 10 fold higher than the suggested threshold. In fact, all of the measured conductance values were an order of magnitude higher than the suggested minimum. In the future, when testing the cortical scaffolds in an animal model, we can expect that vascularization and the formation of osteoid tissues will likely be attained [30].

This study demonstrated osteoid like ECM formation in artificial microchannels. This was seen without the use of a bioreactor and artificial fluid flow and thus the tissue formation was seen close to the surface of the microchannels. However, when the scaffolds were analyzed for cell orientation, cells were seen to uniformly coat the wall surfaces. The osteoid formation in the microchannels was significantly influenced by the number of cell seedings on the scaffolds as well as the total time in culture. The material used to fabricate the scaffolds was not found to affect the osteon like ECM deposition. The same trend of matrix deposition was seen in both osteon area and in the osteon width within channels. Specifically, the matrix synthesis over time within the single seeding group was not significant. This was an expected finding since the cell culture was exposed to dexamethasone, which is a glucocorticoid steroid that promotes osteoblast progenitor differentiation and stops proliferation. Matrix synthesis was markedly different for the multiple seeded groups. Consistent increases in osteonal area were seen up to day 24, whereas osteonal width only increased up to day 18, with a sudden decrease at day 24. This was likely due to bridge formation within the microchannels, which accounted for high surface area, but relatively low osteon thickness. Growth of cells inside microchannels is normally investigated inside tissue engineered scaffolds for blood vessel substitutes [47], in which epithelial cells attach on the walls of a scaffold to recreate the original blood vessels [48]. The experiment described in this research has not previously been shown on such a micro patterned level. In fact, the average blood vessel scaffolds measure at least a few millimeters in diameter [47], so the acting forces, the micro environment and the findings were not fully representative of this research. Other cell matrix synthesis studies inside microchannels do not involve a full 3D substrate, but rather grooves in a substrate material as seen in an article by Holtaus et al., in which microgrooves were developed using a micro molding technique on HAp to investigate cellular orientation [49]. This work represents an initial study using the novel scaffold platform developed to study the effect

of local scaffold micropatterning in the form of channels instead of beams [50] on tissue morphogenesis.

Nano mechanical testing of the ECM deposited inside the microchannels was also performed to determine the influence of the materials tested and cell seedings on the ECM. Microhardness values at day 24 showed that the type of CaP powder used had a significant effect on ECM synthesis. Specifically, the ECM grown in the BCaP scaffolds had significantly higher microhardness than that deposited in HAp substrates. It is possible that higher hardness values were due to higher degrees of mineralization of the extracellular matrix. These findings correlated with the material degradation studies, which showed that day 7 calcium released levels not to be significantly different between HAp and BCaP. However, comparing the predicted calcium release for the HAp and BCaP at day 24, it was speculated that the BCaP's ECM was found to have higher microhardness values potentially due to the elevated $[\text{Ca}^{2+}]$ that was available for the osteoblasts to initiate mineralization. Further evidence included the ratio of BCaP hardness to HAp hardness (single: 2.42; multiple: 2.27) showed a similar trend to the ratio of BCaP Ca^{2+} release to the HAp Ca^{2+} release (1.73) at day 24 of the study but requires validation to prove correlation. The second value measured from the nano indentation was the elastic modulus of the ECM. Neither the scaffold material nor the number of cell seedings demonstrated an impact on the ECM modulus. However, it was observed that the BCaP scaffolds had slightly higher modulus values. In a previous study by our group [51], the ECM was tested on the surface of micropatterned disks with cross sectional microchannels of different diameter. The nano mechanical findings in this study were comparable to those in this concave disk study further underlying that the observed effect is attributable to the underlying substrate curvature. The hardness of the deposited ECM of the 250 μm microchannel diameter disk was $0.76 \pm 0.14 \text{ GPa}$, which was comparable to $0.80 \pm 0.20 \text{ GPa}$ and $0.778 \pm 0.196 \text{ GPa}$ for the single and multiple seeding groups, respectively. The same was valid for the modulus values, in which the concave disk substrate measured at $21.46 \pm 2.33 \text{ GPa}$ and the 3D scaffolds measured at $18.69 \pm 3.70 \text{ GPa}$ (single seeding) and $19.49 \pm 8.42 \text{ GPa}$ (multiple seeding). For comparison, the hardness values of previously reported human bone samples range between 0.47 and 0.74 GPa [36,52–55]. The experimental values from this research were of a slightly higher hardness than what has been previously reported for the reduced elastic modulus of dehydrated human bone, which was 12.40 GPa [36,52–55]. It was hypothesized that the reason this group tested above cortical bone average was because the experimental setup in this study allowed us to measure modulus and hardness directly on the surface of the osteon lamellae.

5. Conclusions

Overall, in this study it was demonstrated that it was possible to recreate cortical bone like scaffold architecture that was consistent, reproducible and could be well characterized. It was also determined that microchannels created using stainless steel needles were very consistent and had high fluid perfusion and conductance. Strong evidence of osteon like organization and mineral deposition was also observed *in vitro*.

Moreover, it was determined that the BCaP material was preferred over the HAp because of both the higher degradation profile and also because it may increase the availability of Ca^{2+} to osteoblasts during osteoid formation for mineralization, which demonstrated improved hardness of the ECM. Apart from affecting the quality of the ECM deposition, material properties were not found to have any other effects on osteoid growth. It was determined that multiple cell seedings, as well as duration of *in vitro* culture, have a significant role in increasing the size of the osteoid matrix synthesis within the channels. In summary, results indicated that the cortical microchannel scaffolds show the appropriate initial mechanical and transport properties, as well as *in vitro* cell response to suggest their suitability to be tested for load bearing graft applications in pre clinical models.

Acknowledgments

This study was supported in part by the UT System South Texas Technology Management (STTM) POC Sparc grant program.

References

- [1] B.R. Martin, D.B. Burr, N.A. Sharkey, *Skeletal Tissue Mechanics*, Springer-Verlag, New York, 1998.
- [2] NIAMS, in: NIH (Ed.), *Scientists Gain New Clues to Bone Mineralization*, 2006.
- [3] W.E. Teo, S. Liao, C. Chan, et al., Fabrication and characterization of hierarchically organized nanoparticle-reinforced nanofibrous composite scaffolds, *Acta Biomater.* 7 (2011) 193–202.
- [4] C.B. Carter, *Norton MG Ceramic Materials: Science and Engineering*, Springer, New York, 2007.
- [5] I. Drosse, E. Volkmer, R. Capanna, et al., Tissue engineering for bone defect healing: an update on a multi-component approach, *Injury* 39 (Suppl. 2) (2008) S9–S20.
- [6] A.J. Wagoner Johnson, B.A. Herschler, A review of the mechanical behavior of CaP and CaP/polymer composites for applications in bone replacement and repair, *Acta Biomater.* 7 (2011) 16–30.
- [7] S.I. Roohani-Esfahani, C.R. Dunstan, J.J. Li, et al., Unique microstructural design of ceramic scaffolds for bone regeneration under load, *Acta Biomater.* 9 (6) (2013) 7014–7024.
- [8] D.W. Huttmacher, Scaffolds in tissue engineering bone and cartilage, *Biomaterials* 21 (2000) 2529–2543.
- [9] S. Bhumiratana, W.L. Grayson, A. Castaneda, et al., Nucleation and growth of mineralized bone matrix on silk-hydroxyapatite composite scaffolds, *Biomaterials* 32 (2011) 2812–2820.
- [10] C. Wu, Y. Zhang, Y. Zhu, et al., Structure–property relationships of silk-modified mesoporous bioglass scaffolds, *Biomaterials* 31 (2010) 3429–3438.
- [11] H. Zhou, Nanoscale hydroxyapatite particles for bone tissue engineering, *Acta Biomater.* 7 (2011) 2769–2781.
- [12] C.E. Tanase, M.I. Pupa, L. Verestiuc, Biomimetic bone scaffolds based on chitosan and calcium phosphates, *Mater. Lett.* 65 (2011) 1681–1683.
- [13] F. Yang, W. Cui, Z. Xiong, et al., Poly(l, l-lactide-co-glycolide)/tricalcium phosphate composite scaffold and its various changes during degradation in vitro, *Polym. Degrad. Stabil.* 91 (2006) 3065–3073.
- [14] H. Cao, N. Kuboyama, A biodegradable porous composite scaffold of PGA/ β -TCP for bone tissue engineering, *Bone* 46 (2010) 386–395.
- [15] Y. Yang, Y. Zhao, G. Tang, et al., In vitro degradation of porous poly(l-lactide-co-glycolide)/ β -tricalcium phosphate (PLGA/ β -TCP) scaffolds under dynamic and static conditions, *Polym. Degrad. Stabil.* 93 (2008) 1838–1845.
- [16] Y. Kang, A. Scully, D.A. Young, et al., Enhanced mechanical performance and biological evaluation of a PLGA coated β -TCP composite scaffold for load-bearing applications, *Eur. Polym. J.* 47 (2011) 1569–1577.
- [17] L. Bakhtiari, H.R. Rezaie, S.M. Hosseinalipour, et al., Investigation of biphasic calcium phosphate/gelatin nanocomposite scaffolds as a bone tissue engineering, *Ceram. Int.* 36 (2010) 2421–2426.
- [18] S. Bose, S. Tarafder, Calcium phosphate ceramic systems in growth factor and drug delivery for bone tissue engineering: a review, *Acta Biomater.* 8 (2012) 1401–1421.
- [19] S.-I. Roohani-Esfahani, The influence hydroxyapatite nanoparticle shape and size on the properties of biphasic calcium phosphate scaffolds coated with hydroxyapatite-PCL composites, *Biomaterials* 31 (2010) 5498–5509.
- [20] H.R.R. Ramay, M. Zhang, Biphasic calcium phosphate nanocomposite porous scaffolds for load-bearing bone tissue engineering, *Biomaterials* 25 (2004) 5171–5180.
- [21] J.A. Puértolas, J.L. Vadillo, S. Sánchez-Salcedo, et al., Compression behaviour of biphasic calcium phosphate and biphasic calcium phosphate–agarose scaffolds for bone regeneration, *Acta Biomater.* 7 (2011) 841–847.
- [22] S.I. Roohani-Esfahani, Z.F. Lu, J.J. Li, et al., Effect of self-assembled nanofibrous silk/polycaprolactone layer on the osteoconductivity and mechanical properties of biphasic calcium phosphate scaffolds, *Acta Biomater.* 8 (2012) 302–312.
- [23] M. Cicuéndez, I. Izquierdo-Barba, S. Sánchez-Salcedo, et al., Biological performance of hydroxyapatite–biopolymer foams: in vitro cell response, *Acta Biomater.* 8 (2) (February 2012) 802–810.
- [24] A. Nemati Hayati, H.R. Rezaie, Hosseinalipour SM Preparation of poly(3-hydroxybutyrate)/nano-hydroxyapatite composite scaffolds for bone tissue engineering, *Mater. Lett.* 65 (2011) 736–739.
- [25] Z.-L. Mou, L.-J. Zhao, Q.-A. Zhang, et al., Preparation of porous PLGA/HA/collagen scaffolds with supercritical CO₂ and application in osteoblast cell culture, *J. Supercrit. Fluids* 58 (2011) 398–406.
- [26] K.H. Tan, C.K. Chua, K.F. Leong, et al., Scaffold development using selective laser sintering of polyetheretherketone–hydroxyapatite biocomposite blends, *Biomaterials* 24 (2003) 3115–3123.
- [27] P. Fabbri, V. Cannillo, A. Sola, et al., Highly porous polycaprolactone–4555 Bioglass® scaffolds for bone tissue engineering, *Compos. Sci. Technol.* 70 (2010) 1869–1878.
- [28] C. Choong, J.T. Triffitt, Z.F. Cui, Polycaprolactone scaffolds for bone tissue engineering: effects of a calcium phosphate coating layer on osteogenic cells, *Food Bioprod. Process.* 82 (2004) 117–125.
- [29] T. Guda, M. Appleford, S. Oh, et al., A cellular perspective to bioceramic scaffolds for bone tissue engineering: the state of the art, *Curr. Top. Med. Chem.* 8 (2008) 290–299.
- [30] P.W. Hui, P.C. Leung, A. Sher, Fluid conductance of cancellous bone graft as a predictor for graft–host interface healing, *J. Biomech.* 29 (1996) 123–132.
- [31] S.K. Nandi, S. Roy, P. Mukherjee, et al., Orthopaedic applications of bone graft & graft substitutes: a review, *Indian J. Med. Res.* 132 (2010) 15–30.
- [32] F. He, J. Ye, In vitro degradation, biocompatibility, and in vivo osteogenesis of poly(lactide-co-glycolic acid)/calcium phosphate cement scaffold with unidirectional lamellar pore structure, *J. Biomed. Mater. Res. A* 100A (12) (December 2012) 3239–3250.
- [33] M.P. McKinley, V.D. O’Loughlin, *Human Anatomy*, McGraw-Hill Higher Education, Boston, 2006.
- [34] M.R. Appleford, S. Oh, J.A. Cole, et al., Effects of trabecular calcium phosphate scaffolds on stress signaling in osteoblast precursor cells, *Biomaterials* 28 (2007) 2747–2753.
- [35] L.A. Schneider, Influence of pH on wound-healing: a new perspective for wound-therapy? *Arch. Dermatol. Res.* 298 (2007) 413–420.
- [36] G.J. Kazakia, E.A. Nauman, D.M. Ebenstein, et al., Effects of in vitro bone formation on the mechanical properties of a trabeculated hydroxyapatite bone substitute, *J. Biomed. Mater. Res. A* 77A (2006) 688–699.
- [37] G.M. Oliver WCaP, An improved technique for determining hardness and elastic modulus using load and displacement sensing indentation experiments, *J. Mater. Res.* 7 (1992) 1564–1583.
- [38] E.K.F. Yim, R.M. Reano, S.W. Pang, et al., Nanopattern-induced changes in morphology and motility of smooth muscle cells, *Biomaterials* 26 (2005) 5405–5413.
- [39] S. Maeno, Y. Niki, H. Matsumoto, et al., The effect of calcium ion concentration on osteoblast viability, proliferation and differentiation in monolayer and 3D culture, *Biomaterials* 26 (2005) 4847–4855.
- [40] S.-J. Ding, C.-W. Wang, D.C.-H. Chen, et al., In vitro degradation behavior of porous calcium phosphates under diametral compression loading, *Ceram. Int.* 31 (2005) 691–696.
- [41] L. Boilet, M. Descamps, E. Rguiti, et al., Processing and properties of transparent hydroxyapatite and β tricalcium phosphate obtained by HIP process, *Ceram. Int.* 39 (1) (2013) 283–288.
- [42] J. Chen, Y. Wang, X. Chen, et al., A simple sol-gel technique for synthesis of nano-structured hydroxyapatite, tricalcium phosphate and biphasic powders, *Mater. Lett.* 65 (2011) 1923–1926.
- [43] A. Farzadi, M. Solati-Hashjin, F. Bakhshi, et al., Synthesis and characterization of hydroxyapatite/ β -tricalcium phosphate nanocomposites using microwave irradiation, *Ceram. Int.* 37 (2011) 65–71.
- [44] K. Kurashina, H. Kurita, Q. Wu, et al., Ectopic osteogenesis with biphasic ceramics of hydroxyapatite and tricalcium phosphate in rabbits, *Biomaterials* 23 (2002) 407–412.
- [45] F. Monchau, A. Lefèvre, M. Descamps, et al., In vitro studies of human and rat osteoclast activity on hydroxyapatite, β -tricalcium phosphate, calcium carbonate, *Biomol. Eng.* 19 (2002) 143–152.
- [46] S. Yamada, D. Heymann, J.M. Boulter, et al., Osteoclastic resorption of calcium phosphate ceramics with different hydroxyapatite/ β -tricalcium phosphate ratios, *Biomaterials* 18 (1997) 1037–1041.
- [47] X. Hu, H. Shen, F. Yang, et al., Preparation and cell affinity of microtubular orientation-structured PLGA(70/30) blood vessel scaffold, *Biomaterials* 29 (2008) 3128–3136.
- [48] P.-H. Lee, S.-H. Tsai, L. Kuo, et al., A prototype tissue engineered blood vessel using amniotic membrane as scaffold, *Acta Biomater.* 8 (9) (Sep 2012) 3342–3348.
- [49] M.G. Holthaus, J. Stolle, L. Treccani, et al., Orientation of human osteoblasts on hydroxyapatite-based microchannels, *Acta Biomater.* 8 (2012) 394–403.
- [50] K.F. Leong, C.M. Cheah, C.K. Chua, Solid freeform fabrication of three-dimensional scaffolds for engineering replacement tissues and organs, *Biomaterials* 24 (2003) 2363–2378.
- [51] M. Pilia, *Tissue Engineered Scaffold for Lamellar Bone Regeneration Biomedical Engineering*, University of Texas at San Antonio, San Antonio, TX, 2012.
- [52] J.Y. Rho, T.Y. Tsui, G.M. Pharr, Elastic properties of human cortical and trabecular lamellar bone measured by nanoindentation, *Biomaterials* 18 (1997) 1325–1330.
- [53] J.-Y. Rho, M.E. Roy, T.Y. Tsui, et al., Elastic properties of microstructural components of human bone tissue as measured by nanoindentation, *J. Biomed. Mater. Res.* 45 (1999) 48–54.
- [54] M.E. Roy, J.-Y. Rho, T.Y. Tsui, et al., Mechanical and morphological variation of the human lumbar vertebral cortical and trabecular bone, *J. Biomed. Mater. Res.* 44 (1999) 191–197.
- [55] C.H. Turner, J. Rho, Y. Takano, et al., The elastic properties of trabecular and cortical bone tissues are similar: results from two microscopic measurement techniques, *J. Biomech.* 32 (1999) 437–441.